JACS
JOURNAL OF THE AMERICAN CHEMICAL SOCIETY
Article
pubs.acs.org/JACS

Monitoring Mechanistic Details in the Synthesis of Pyrimidines via Real-Time, Ultrafast Multidimensional NMR Spectroscopy

Zulay D. Pardo,[‡] Gregory L. Olsen,[†] María Encarnación Fernández-Valle,[§] Lucio Frydman,*[,†] Roberto Martínez-Álvarez,[‡] and Antonio Herrera*[,‡,§]

[†]Department of Chemical Physics, Weizmann Institute of Science, 76100 Rehovot, Israel

[‡]Departamento de Química Orgánica I and [§]CAI de RMN y RSE, Facultad de Ciencias Químicas, Universidad Complutense, 28040 Madrid, Spain

Supporting Information

ABSTRACT: Recent years have witnessed unprecedented advances in the development of fast multidimensional NMR acquisition techniques. This progress could open valuable new opportunities for the elucidation of chemical and biochemical processes. This study demonstrates one such capability, with the first real-time Two-dimensional (2D) dynamic analysis of a complex organic reaction relying on unlabeled substrates. Implementing such measurements required the development of new ultrafast 2D methods, capable of monitoring multiple spectral regions of interest as the reaction progressed. The alternate application of these acquisitions in an interleaved, excitation-optimized fashion, allowed us to extract new structural and dynamic insight concerning the reaction between aliphatic ketones and triflic anhydride in the presence of nitriles to yield alkylpyrimidines. Up to 2500 2D NMR data sets were thus collected over the course of this nearly 100 min long reaction, in an approach resembling that used in functional magnetic resonance imaging. With the aid of these new frequency-selective low-gradient strength experiments, supplemented by chemical shift calculations of the spectral coordinates observed in the 2D heteronuclear correlations, previously postulated intermediates involved in the alkylpyrimidine formation process could be confirmed, and hitherto undetected ones were revealed. The potential and limitations of the resulting methods are discussed.

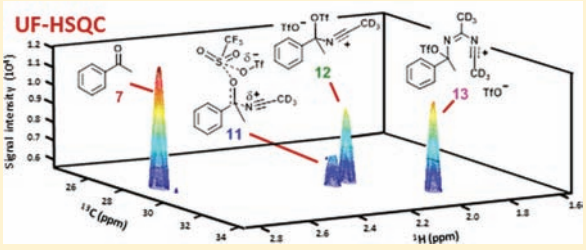

1. INTRODUCTION

Heterocycles' significance is central in modern chemistry.[1] Among nitrogen-containing heterocycles, pyrimidines play unique roles as integral constituents in many pharmaceutical, functional, and natural materials.[2] Understanding and controlling laboratory preparations of pyrimidinic derivatives have therefore become an important field of synthetic chemistry.[3] Recently we focused our attention on one-pot syntheses of various heterocyclic derivatives and developed alternatives for an easier preparation of a wide range of azaheterocyclic compounds.[4] Other elegant procedures have been also described for the synthesis of pyrimidine derivatives[5] and oxazoles.[6] Several of these studies revealed details of the mechanism of pyrimidine formation when reacting carbonyl compounds with strong electrophiles, such as trifluoromethanesulfonic acid anhydride (triflic anhydride, Tf_2O).[7] Still, despite the importance of these reactions, large gaps in knowledge remain about the variety of intermediates and mechanistic routes involved in their formation, and key details about the structural information associated to the kinetics of these processes remain to be elucidated.

Real-time NMR measurements could open unique opportunities in the analysis of complex chemical problems such as this one. Two-dimensional (2D) NMR, in particular, could enable one to monitor and assign transient intermediates in the reaction as well as to quantify their overall kinetics of formation. Doing so, however, requires completing the 2D NMR measurement in time scales compatible with the chemical changes occurring following a sudden triggering of the reaction. Much progress has taken place during recent years in the area of accelerating multidimensional NMR—both in the areas of organic and biomolecular acquisitions. Efforts that have made 2D spectroscopy compatible with the tracking of rapid transformations include Hadamard-encoded versions of heteronuclear (HSQC) and homonuclear (TOCSY) NMR exploiting a priori information,[8] compressed sensing acquisitions where the usual Nyquist demands for the FT-based sampling of a NMR domain can be alleviated,[9] and so-called "ultrafast" (UF) acquisition schemes whereby arbitrary 2D NMR correlations can be established in a single-scan fashion.[10] The latter approach in particular replaces the indirect-domain parametric time encoding of 2D NMR with a spatiotemporal manipulation, effectively imparting all the increments that would be involved in a conventional experiment—in their entirety—within one single scan.[11] The spatial patterns imparted by indirect domain evolution frequencies encoded in such a manner can be subsequently read out with the aid of suitable magnetic field

Received: October 28, 2011
Published: January 4, 2012

dx.doi.org/10.1021/ja210154g | J. Am. Chem.Soc. 2012, 134, 2706–2715

gradients. Using such rapid acquisition 2D NMR methods, a number of fast-reacting systems have been recently monitored in real time. These have included biomolecular single- and multiple-quantum heteronuclear correlations (HSQC and HMQC) on proteins and nucleic acids[12] as well as TOCSY and multiple-bond correlation experiments on reacting organic systems.[13a] Included among the latter were studies on the synthesis of alkyl- and alkylaryl-pyrimidines from aliphatic and aromatic ketones, whereby series of complete 2D NMR data sets were collected on 100% abundant isotopes to observe the changes in chemical species occurring as the reactions progressed.

We have recently studied these reactions for the specific case of the addition of 3-pentanone **1** to acetonitrile-d_3 in the presence of triflic anhydride (Scheme 1). In these studies 2D

Scheme 1

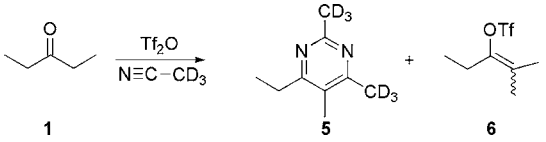

1 5 6

ultrafast TOCSY homonuclear acquisitions revealed the presence of intermediates **2**–**4**, and the generation of the final reaction products **5** and **6** was revealed (Scheme 2).[13b] Two-dimensional ultrafast heteronuclear multiple bond correlation spectroscopy (HMBC) experiments on specifically labeled precursors were also implemented to elucidate the chemical nature and evolution of reactive quaternary centers involved in this reaction. Upon monitoring a similar condensation that starting from ^{13}C-carbonyl-labeled acetophenone **7** lead to alkylaryl-pyrimidine **9** as main product (Scheme 3), such experiments permitted the detection of the intermediate (trifluorormethylsulfonyloxy)carbenium ion **8**.[13c]

Unfortunately, label-based experiments such as these have a narrow focus that may obscure a full and unambiguous identification of all transient intermediates generated during the course of the reaction. To extract such important mechanistic information, it would be necessary to implement more general 2D NMR correlations. Particularly useful could be site-identifying heteronuclear correlations covering the full possible range of chemical shifts that might arise, so that both permanent as well as transient species can be characterized. Running ultrafast HSQC experiments at natural abundance in non-labeled samples, however, would not be a trivial endeavor. Indeed in single scan sequences, the spectral widths SW_2 and SW_1 along the directly and indirectly sampled dimensions are related to one another. Moreover these parameters as well as the effective spectral resolution $\Delta\nu_1$ desired along the indirect domain define the gradient strength G_a required to read out the indirect domain spectral width according to $(SW_1SW_2)/(\Delta\nu_1) \sim \gamma_a G_a L$, where L is the encoded sample length. The per scan signal-to-noise ratio (SNR) is in turn also governed by the $\gamma_a G_a L$ frequency span, which becomes the filter bandwidth that needs to be used for this kind of measurement. Noise in this kind of experiment thereby behaves proportionally to $\sqrt{(SW_1 \cdot SW_2/\Delta\nu_1)}$. For the kind of HSQC and HMBC experiments that would be needed to characterize a priori unknown intermediates that can fall anywhere in the aliphatic/olefinic/aromatic range, as is the case for the kind of reaction depicted in Scheme 3, this relation would impose high strains on the gradient strengths that would be necessary (≈80 G/cm for covering an indirect domain spanning ≈150 ppm, a direct domain of ≈4 kHz, and the typical 1.8 cm sample length). Even worse, the associated noise penalties would become untenable for the ensuing kind of filter bandwidths.

One of the aims of this work consisted in developing a methodology which would allow us to monitor the necessary spectral widths while bypassing such stringent demands. Strategies have been discussed in the recent literature capable of alleviating the gradient strengths needed to decode a given spectral bandwidth in single-scan 2D NMR, including the folding of peaks along the direct and indirect domain as well as shifting of peaks into a single, congruent band of detection.[14] In the present instance, however, we decided to explore an alternative route that, while still alleviating the gradient's demands, could still furnish a direct reading of the chemical shift information about the transient reaction intermediates. To do so a new family of experiments was devised incorporating (i) the selective excitation of different spectral bands of interest (aliphatic, olefinic, aromatic) and (ii) the interleaving of real-time ultrafast acquisitions targeting these spectral bands through consecutive scans. With the aid of such strategies it was possible to interrogate the nature of the chemical dynamics in Scheme 3 using unlabeled compounds, recording literally thousands of 2D heteronuclear correlation spectra within the course of these hour-long processes. With the aid of such data, of ancillary 1D NMR measurements, and of computer-based estimators of chemical shift values, new transient intermediates were detected, and their kinetics of generation/consumption characterized. All this led us to propose a new two-pathway mechanism for the triflate-mediated addition of acetonitrile-d_3 to arylketones.

2. MATERIALS AND METHODS

To address the spectral-width/spectral-resolution issues just mentioned, we decided to attempt the observation of the reaction in Scheme 3 at natural abundance by modifying a general, broadband heteronuclear correlation experiment, into a multiple-window observation mode. In other words, instead of implementing ultrafast sequences covering in excess of 100 ppm in the ^{13}C domain, the targeted direct- and indirect-domain windows were split into regions expected to possess the peaks of interest. Areas that were a priori, known to be devoid of peaks, were consequently ignored. Moreover, these multiple spectrally selective versions of single-bond heteronuclear correlation ultrafast sequences were run in an interleaved fashion so as to employ the relaxation recovery delay of one spectral

Scheme 2

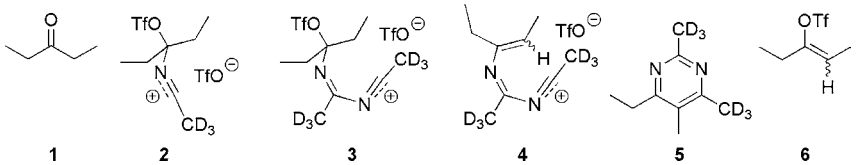

1 2 3 4 5 6

dx.doi.org/10.1021/ja210154g | J. Am. Chem.Soc. 2012, 134, 2706–2715

Scheme 3

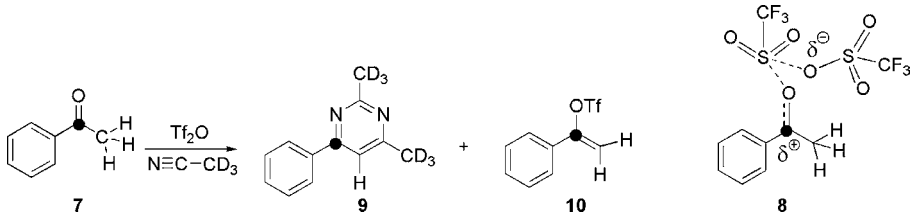

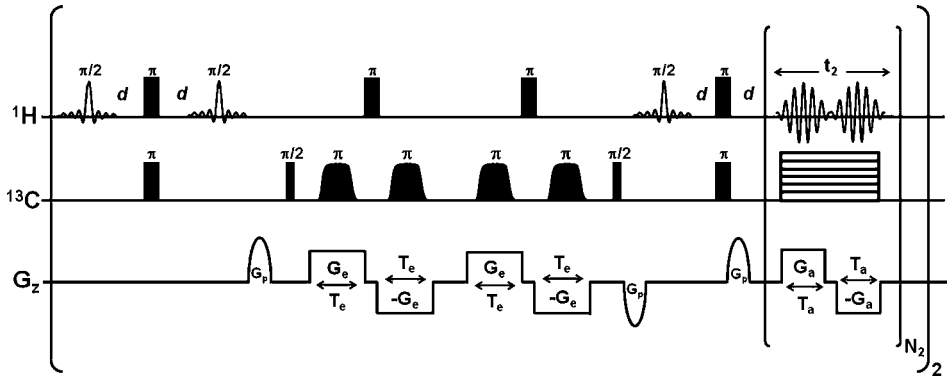

Figure 1. Multiwindowed ultrafast HSQC pulse sequence involving: a selective excitation of protons in the targeted spectral window; an INEPT magnetization transfer to carbon; four chirped pulses applied in the presence of suitable gradients and $(\pi)^{H}$ decoupling pulses to give a constant-time spatial encoding of the carbon evolution; a selective transfer of this encoded information to protons; and low-strength $\pm G_a$ gradient pairs acting as read-out of the resulting encoded signals. After shifting the irradiation frequencies to a second spectral window, the sequence is then immediately repeated to acquire a second FID addressing a different spectral region. Selective excitation and spatial encoding used 1.42 ms sinc $\pi/2$ pulses and 2.5 ms π chirp pulses, respectively. Encoding gradient strengths were 25 G/cm. Read out of encoded signals typically used N_2 =40 cycles and a G_a of 6.35 or 10.6 G/cm. The narrow independent windows targeting specific spectral regions of interest permits use of these low-strength gradients, providing corresponding increases in SNR and enabling the detection of nonlabeled samples.

region to collect the data pertaining to another spectral region—very much like multislice imaging experiments perform their optimized acquisitions in frecuency-shifted 3D MRI.[15] To do so in the ultrafast instances, care had to be made to either avoid the excitation of ^{1}H signals outside the targeted region or, alternatively, to make sure that unencoded regions were addressed by an even number of $(\pi)^{H}$ rotations so as to return their magnetizations to a relaxation-optimized longitudinal state. (^{13}C manipulations being less critical for all cases given that ^{1}H initiated, indirectly detected sequences were assayed.) Three spectral windows were selected for these observations, usually involving ≈1.5 ppm along the ^{1}H and ≈10−20 ppm along the ^{13}C dimension. These windows encompassed: (i) an 'aliphatic' region centered at 2.2 ppm (^{1}H) and 28.7 ppm (^{13}C); (ii) an 'olefinic' region at 5.8 ppm (^{1}H) and 110.9 ppm (^{13}C) set to follow transient intermediates; and (iii) an aromatic 'pyrimidinic' region centered at 8.2 ppm (^{1}H) and 117.4 ppm (^{13}C) to track formation of the final reaction product 2,4-dimethyl-6-phenylpyrimidine-d_6 (**9**). A typical scheme of these pulse sequences is illustrated in Figure 1. This consists of a series of back-to-back heteronuclear correlations involving two continuous constant-time spatial encoding processes for monitoring the indirect domain ^{13}C evolution. As each one of these additive processes involved a $(\pi)^{H}$ decoupling pulse in their center, no overall rotation of the proton magnetizations resulted from the t_1 period. The two INEPT transfers in each of these sequences incorporated sinc$(\pi/2)^{H}$ excitations and two hard $(\pi)^{H}$ pulses, thereby fulfilling the band-selectivity requirements of these sequences. These multiwindowed constant-time ultrafast 2D NMR data sets were collected on a Varian VNMRS 600 MHz NMR spectrometer using a triply tuned HCN single-gradient probe at 298 K. The constant-time spatial encoding adiabatic $(\pi)^{C}$ pulses needed for the spatial encoding were generated using the Varian Pbox software package, with these chirped pulses sweeping a bandwidth $[O_i-O_f]$ = 49 519 Hz in 2.5 ms, applied in conjunction with 25 G/cm encoding gradients. All protons were selectively excited in their appropriate bandwidths with 1.42 ms long, 1 kHz bandwidth $(\pi/2)^{H}$ pulses. All experiments used 180° phase cycling of both the initial $(\pi/2)^{C}$ hard pulse and the receiver phase, for ensuring a more complete suppression of the natural abundance background. Acquisitions used gradient strengths of G_a = 6.35 or 10.6 G/cm and filter bandwidths of either 25 or 42 kHz (as noted in the text). Further acquisition parameters included N_2 = 40 cycles of ± gradient pairs, a physical sampling dwell time of 2 μs, and gradient durations T_a = 0.60 ms each. Square $(\pi)^{C}$ pulses were applied in between all acquisition gradients for heteronuclear decoupling purposes. Purge gradient pulses preceding acquisition were 1.60 ms in duration, at 6.35 G/cm (10.6 G/cm for the experiment using labeled starting material (**7**) to probe the olefinic region).

The reaction described in Scheme 3 was initially monitored using spectral windows spanning 800.8 Hz in ^{1}H and 2500 Hz in ^{13}C. To permit an enhanced sensitivity, the ^{13}C window sizes were further reduced to 1500 Hz in subsequent tests. Gradients and bandwidths were adjusted accordingly, as noted below. Each 0.5 mL acetophenone-acetonitrile solution was pretuned and preshimmed prior to injection of a small aliquot (≈56 μL) of Tf_2O. A mixing device was used for this injection, including a syringe feeding directly into the NMR tube inside the magnet (see Supporting Information). Data collection was initiated prior to injection of Tf_2O. Preliminary tests monitoring ^{13}C-labeled acetophenone (**7**) used two scans per 2D spectrum. Reactions monitoring unlabeled acetophenone (**7**) were acquired using 12 scans per FID and a four-step phase cycle, again with 180° phase cycling of both ^{13}C $\pi/2$ pulses and of the receiver phase. Each double-window HSQC data set thus required 4.16 s per scan when using the 2 s recycle delay. Total times per 2D spectrum were 8.32 and 49.9 s for monitoring of labeled and nonlabeled reactants, respectively. This back-to-back application of separate ultrafast HSQC experiments, targeting different windows of interest, permitted the parallel observation of multiple spectral windows in the same real-time acquisition batch. While as many as four distinct spectral regions were monitored in certain runs, only two windows per experiment (Figure 1) are presented in this work. The resulting concatenated time-domain signals were separated into FIDs corresponding to the individual

dx.doi.org/10.1021/ja210154g | J. Am. Chem.Soc. 2012, 134, 2706−2715

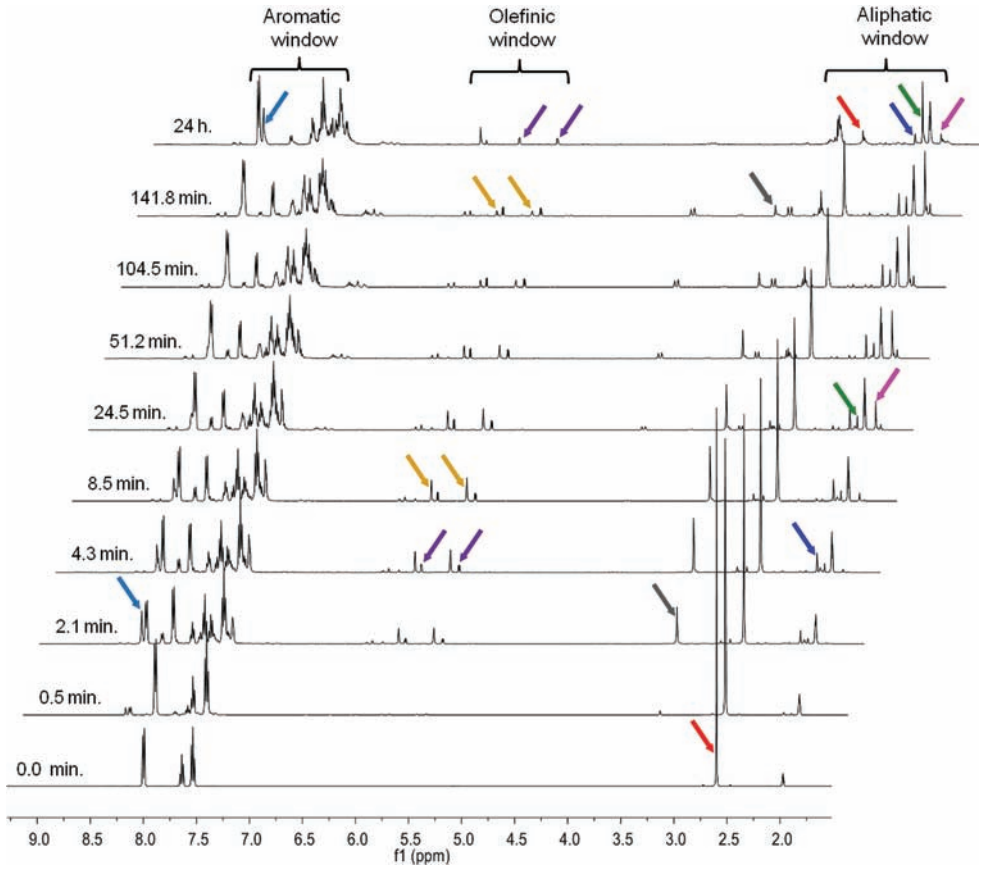

Figure 2. Real-time 1D ^{1}H NMR series recorded as a function of time (only a small subset of the resulting spectra hereby shown). Colored arrows show the positions of specific signals from products and intermediates participating in the reaction between acetophenone (**7**) (0.183 mmol) and triflic anhydride (0.275 mmol) in acetonitrile-d_3 (as both a coreactant and solvent) at 298 K. The red arrow at (2.60 ppm, 0.0 min) indicates the signal of methyl group from starting acetophenone. Light-blue and purple arrows show signals from final products, aromatic proton H-5 (8.32 ppm, 2.1 min) in pyrimidine (**9**), and the methylidene protons (5.85 and 5.49 ppm, 51.2 min) in vinyl triflate (**10**), respectively. Gray (3.28 ppm), blue (2.11 ppm), green (2.04 ppm), and magenta (1.87 ppm) arrows represent the position of methyl group in different aliphatic intermediates; gold (5.90/5.57 ppm) arrows present the positions of methylidene protons from olefinic intermediates as well.

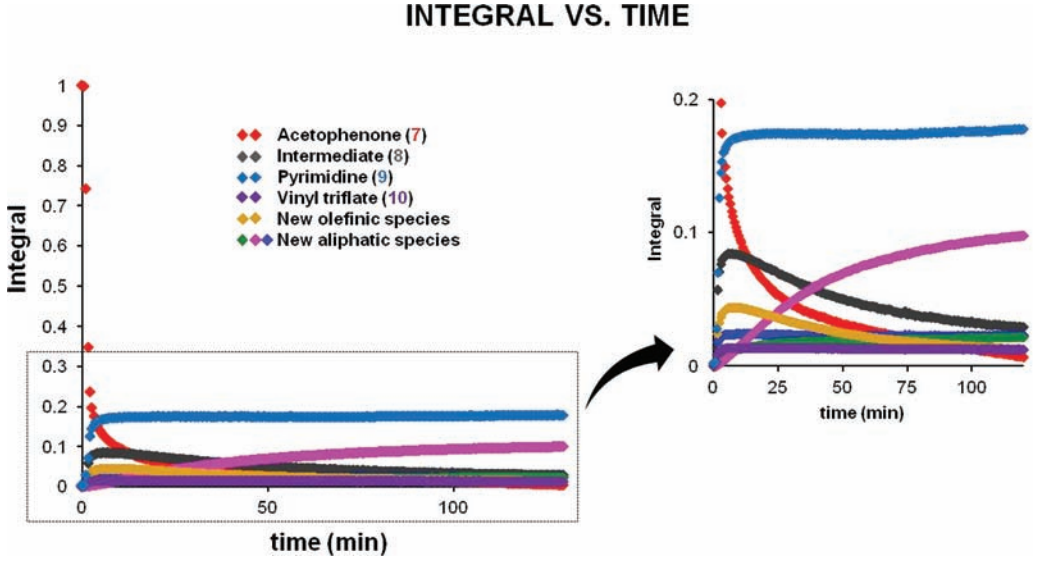

Figure 3. Normalized integrals as a function of time, taken from the real-time 1D ^{1}H NMR series shown in Figure 2. The integrals were measured by taking the characteristic signals for the initial ketone (**7**, red), the final pyrimidine (**9**, light blue), vinyl triflate (**10**, purple), and the intermediate (**8**, gray) as well as for other new intermediates detected in these studies. The right-hand panel presents an expanded description of these compounds' time dependencies.

dx.doi.org/10.1021/ja210154g | J. Am. Chem.Soc. 2012, 134, 2706–2715

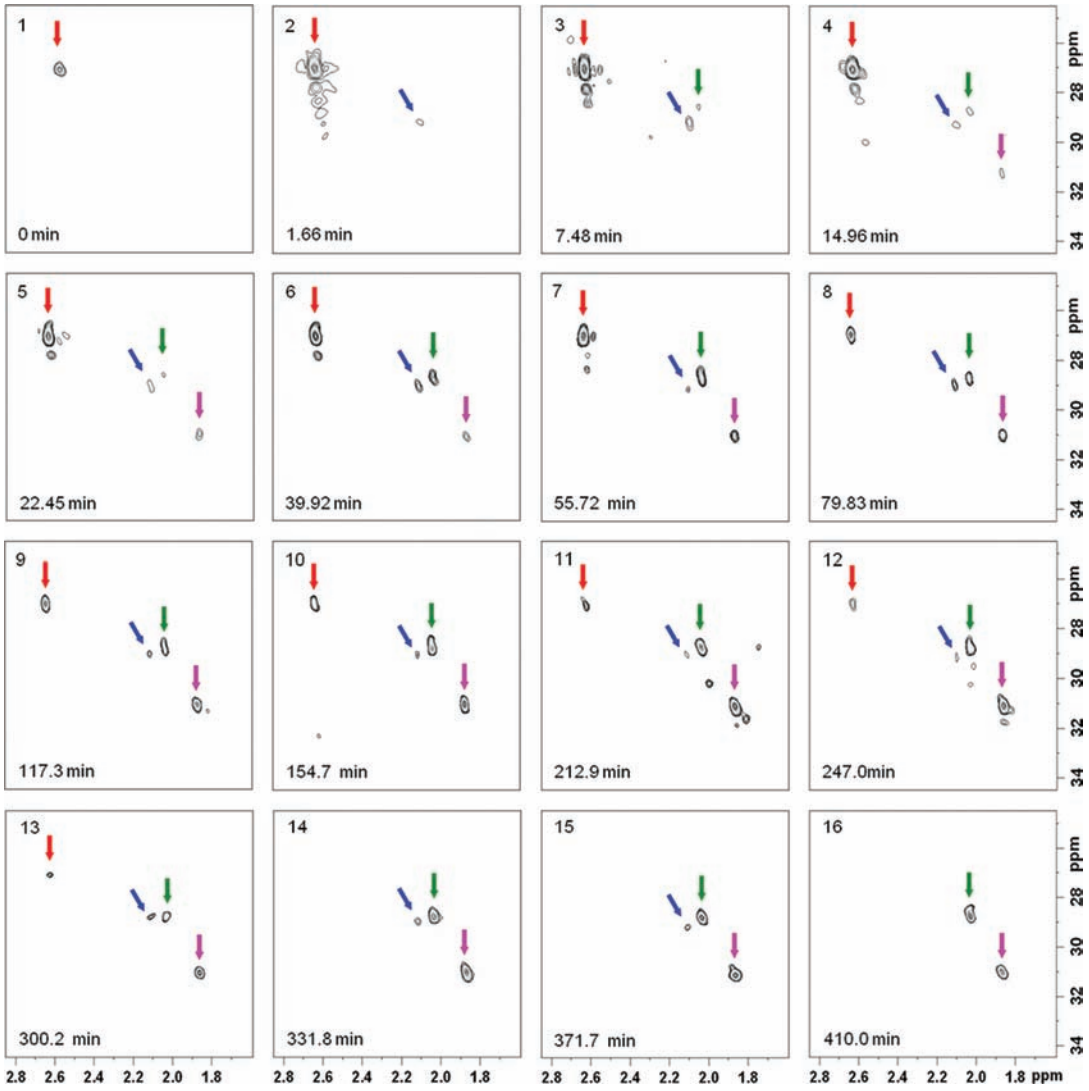

Figure 4. Representative selection of real-time 2D HSQC NMR spectra arising from the reaction of triflic anhydride, ketone (**7**) and acetonitrile-d_3. Spectra show species (**7** and **11**−**13**) present in the aliphatic window range (1.54−2.87 ppm for ^{1}H, 23.7−33.7 ppm for ^{13}C) at key time points as the reaction progressed, depicted by arrows (red, blue, green, and magenta, respectively) (see text for further details).

windows, then processed into 2D spectra in the usual ultrafast fashion, and characterized using custom-written Matlab scripts. To aid in the elucidation of the reaction intermediate structures, ^{1}H NMR chemical shifts were estimated using Advanced Chemistry Development, Inc. (ACD/Laboratories) Software V8.0, and ^{13}C NMR shifts were calculated within the GIAO approximation[16] on the PCM-M06-2X/6-31+G* (solvent = acetonitrile)[17,18] with optimized geometries using the Gaussian 09 suite of programs.[19]

3. RESULTS AND DISCUSSION

3.1. Real-Time 1D Measurements. A variety of preliminary 1D ^{1}H NMR data were taken to delineate the spectral windows to be used for the main 2D studies. Figure 2 illustrates a representative set of such tests. In addition to signals corresponding to reagents and products (Scheme 3), these tests revealed over a dozen transient signals in the ^{1}H aliphatic and olefinic regions. These signals—arising on top of the ^{1}H NMR resonances belonging to reagents and products—suggest the presence of a number of candidate aliphatic and olefinic intermediates that had not been previously noticed. Aliphatic intermediates will be characterized by singlet signals from methyl group present, whereas olefinic intermediates will show doublets produced by the diastereotopic protons from the methylidene group. Figure 3 presents a more quantitative description on the appearance and disappearance of these different species, showing the time-dependent intensities of products **7**, **9**, and **10** as well as of intermediate **8** (cf. Scheme 3). Also shown is the kinetic behavior of an additional number of aliphatic and olefinic intermediates arising during the reaction.

3.2. Ultrafast 2D Heteronuclear Correlations. The identities of the intermediates involved cannot be determined exclusively from 1D ^{1}H NMR experiments. To obtain structural insight into these peaks, real-time ultrafast NMR techniques correlating data from ^{1}H and ^{13}C nuclei were recorded. Based on the temporal series of ^{1}H NMR experiments, three different spectral windows were selected for examination by real-time 2D NMR. One focused on an aliphatic region: 1.54−2.87 ppm for ^{1}H with 23.7−33.7 ppm for ^{13}C; another in an olefinic one: 5.17−6.50 ppm for ^{1}H with 106.0−116.0 ppm for ^{13}C; and a third in an aromatic/pyrimidinic one: 7.49−8.81 ppm for ^{1}H with 112.40−122.40 ppm for ^{13}C. A series of UF-HSQC spectra was taken for each window of interest; they are

dx.doi.org/10.1021/ja210154g | J. Am. Chem.Soc. 2012, 134, 2706−2715

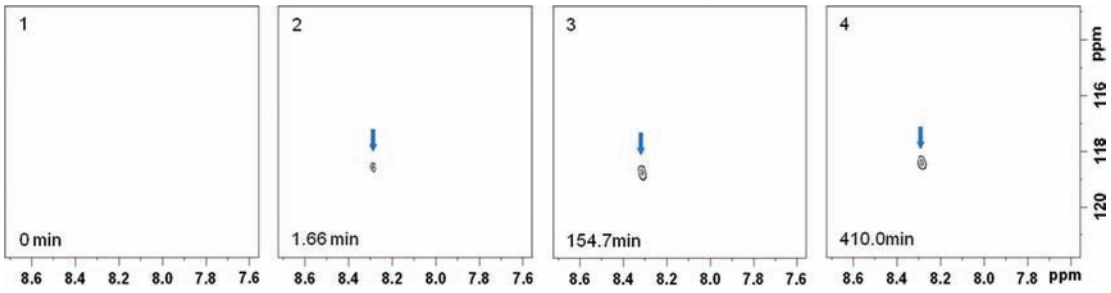

Figure 5. Representative selection of the real-time 2D HSQC NMR spectral series arising from the reaction of triflic anhydride, ketone (**7**), and acetonitrile-d_3. Spectra taken as the reaction progressed show a cross peak (blue arrow) in the aromatic/pyrimidinic window range (7.49−8.81 ppm for ^{1}H, 112.40−122.40 ppm for ^{13}C) arising from the H5−C5 single bond of the pyrimidine (**9**, light-blue arrow) (see text for further details).

illustrated in Figures 4 and 5. Colored arrows in these plots denote cross-peaks representing reagents, products, and intermediates that participate in the reaction. Cross-peaks assigned to starting ketone (**7**) and final products vinyl triflate (**10**) and pyrimidine (**9**) were confirmed by 1D and 2D spectra (see the Supporting Information). Values of chemical shifts of highlighted (bold) nuclei are shown in Scheme 4.

Scheme 4

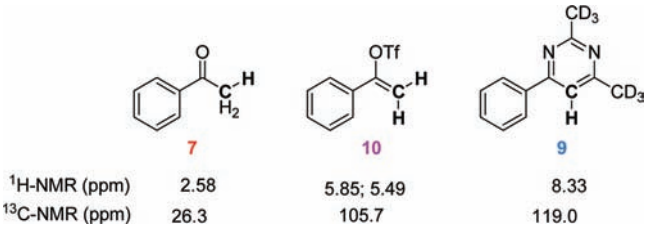

Figure 4 illustrates a series of representative 2D UF-HSQC spectra recorded for the aliphatic window at ca. 30 s delay. A total of 500 HSQC spectra was taken in a typical kinetic progression, where data acquisition was begun immediately prior to the sudden addition of triflic anhydride to a solution of ketone (**7**) in acetonitrile-d_3 (Figure 4 highlights only 16 of these, a full 3D animation made from the total set of HSQC experiments is given as Supporting Information). Prior to the Tf_2O injection, the cross-peak of the methyl group of (**7**) is clearly observed (0 min, red arrow). 1.66 min after initiation of the reaction a new cross-peak at δ = 2.09/28.40 ppm (blue arrow) is seen. Then, at ca. 7.48 and 14.97 min, two additional cross-peaks at 2.02/28.10 ppm (green arrow) and 1.82/30.30 ppm (magenta arrow), respectively, were clearly detected. The intensity of these cross-peaks changed with time, rising and falling during the course of the reaction (see Figure 6).

A series of representative 2D UF-HSQC spectra were recorded in succession on the olefinic window (5.17 - 6.50 ppm, ^{1}H; 106.0 - 116.0 ppm, ^{13}C) and on the aromatic/pyrimidinic region (7.49 - 8.81 ppm, ^{1}H; 112.4 - 122,4 ppm, ^{13}C). Throughout the series of 500 HSQC spectra recorded in these windows, doublet cross-peaks from vinyl triflate (**10**) and olefinic intermediates were not detected. Figure 5 illustrates the 2D heteronuclear correlation observed for the aromatic/pyrimidine window. The spectra for this window are dominated by a cross-peak (8.33/119.0 ppm, light blue arrow) which appears with variable intensity in the aromatic region, corresponding to the H5−C5 single-bond of the pyrimidine (**9**). Its assignment to the pyrimidine (**9**) was confirmed independently by 1D and 2D standard NMR analyses. Figure 6 summarizes the time-evolution of key cross-peaks observed in the various windows studied. The aliphatic window (left) shows the kinetic behavior for reagent acetophenone (**7**) and intermediates (**11**), (**12**), (**13**). The aromatic window (right) reflects the formation of final product pyrimidine (**9**). (A 3D animation showing the complete time-series of spectra for the aromatic window is available for download as Supporting Information).

To further examine the olefinic window, the experiment was repeated with labeled ^{13}C-carbonyl-acetophenone (**7**) as the reagent. A spectral window targeting 5.17−6.50 ppm for ^{1}H and 102.6−119.2 ppm for ^{13}C permitted the observation and

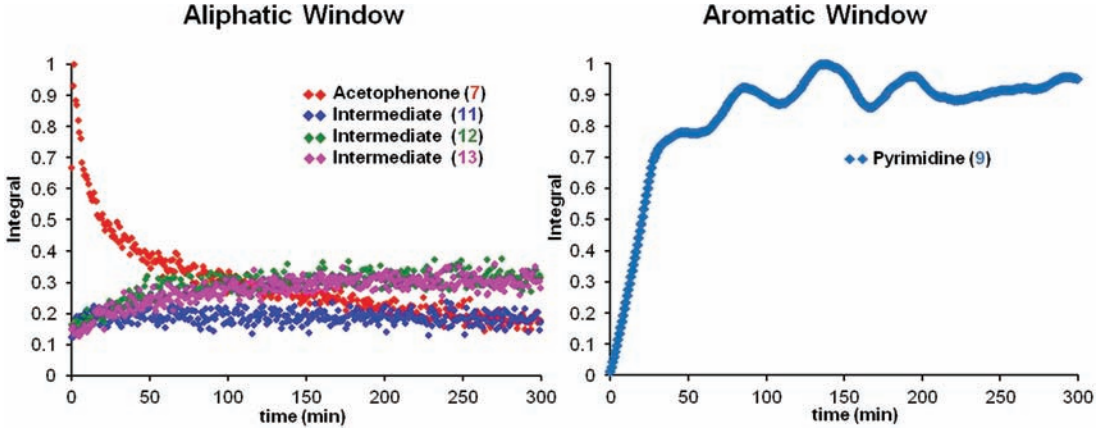

Figure 6. Integral values versus time-evolution of key cross-peaks as observed for the aliphatic and the aromatic windows studied.

dx.doi.org/10.1021/ja210154g | J. Am. Chem.Soc. 2012, 134, 2706−2715

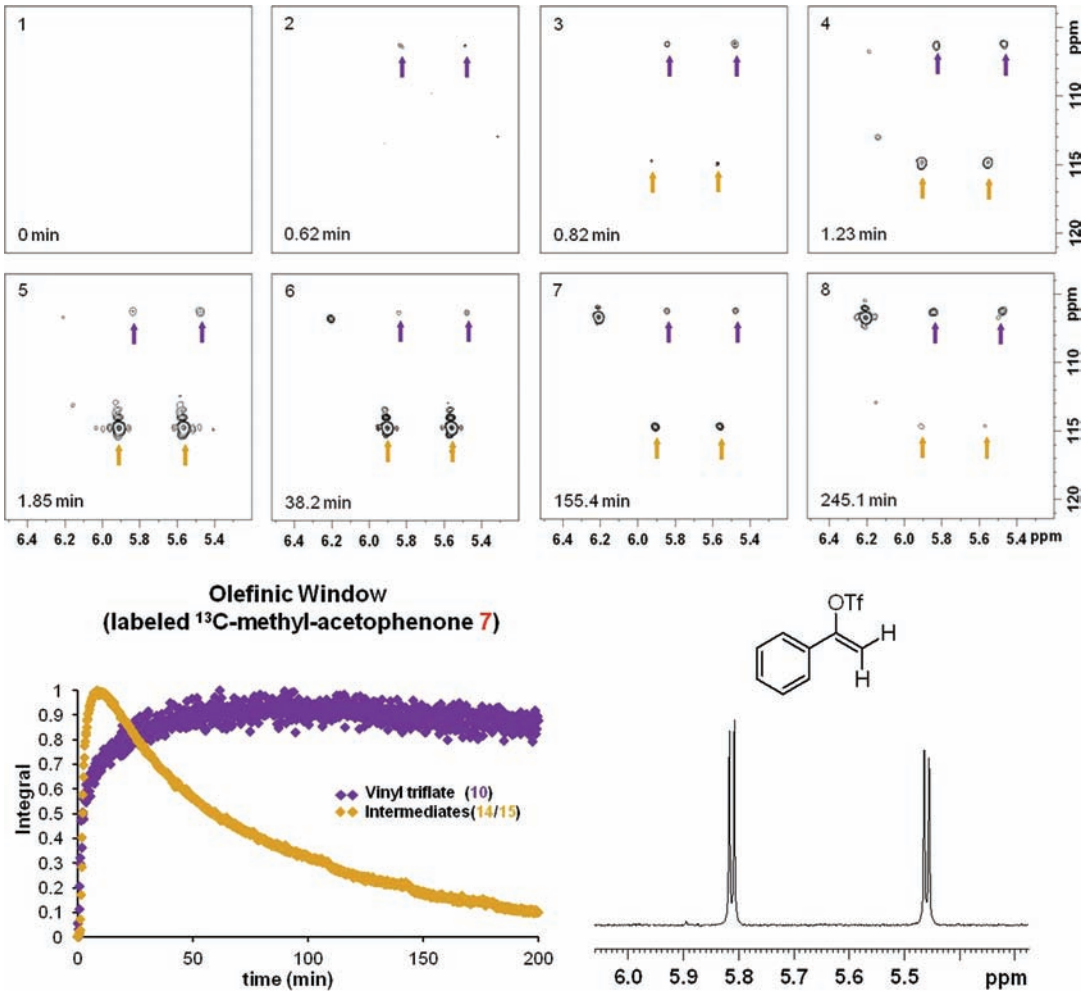

Figure 7. Representative selection of real-time 2D HSQC NMR spectra arising from the reaction of triflic anhydride, labeled ^{13}C-methyl-acetophenone (**7**), and acetonitrile-d_3. Spectra show species (**10**) and (**14**/**15**) present for the olephinic window range (5.17−6.50 ppm ^{1}H, 102.6−119.2 ppm ^{13}C) indicated by purple and dark-yellow arrows, respectively (top). The left bottom panel shows the time-dependent peak intensities (integrals) of the vinyl triflate (**10**) and the newly found intermediates (**14**/**15**) which represent the variation in their respective concentrations during the course of the reaction. The right bottom panel shows the olefinic peaks in a ^{1}H NMR spectrum of isolated and purified vinyl triflate.

comparison of olefinic products and intermediates. A total of 1200 HSQC spectra taken under these conditions within the course of the reaction revealed, in addition to the expected doublet of cross-peaks from vinyl triflate (**10**, purple arrow), a new doublet of cross-peaks (Figure 7). The rise and fall of these cross-peaks (dark-yellow arrows) show its character as intermediate. Figure 7 (bottom) also displays the kinetic behavior of the new olefinic intermediates (**14**) and/or (**15**). Additionally the presence of a time-increasing cross-peak at 6.20/106.5 was observed. As seen in Figure 7, the kinetics of the vinyl triflate (**10**) are in good agreement with those seen initially in the nonlabeled reaction. For a 3D animation see the Supporting Information.

4. DISCUSSION

The time-evolution of the peak intensities observed in the various real-time 1D and 2D spectra illustrated in the preceding section suggest a complex sequence of events underlying the evolution of the starting acetophenone (**7**) to the final pyrimidine (**9**). A mechanism capable of rationalizing all the observed peaks is depicted in Figure 8. The HSQC series recorded on the 1.54−2.87 ppm, ^{1}H, and 23.7−33.7 ppm, ^{13}C aliphatic window, indicates that the reaction starts with an electrophilic attack of the S-atom of one of the SO_2 groups of triflic anhydride on the O-atom of the carbonyl group of acetophenone (**7**) leading to the rapid formation of an intermediate (**8**), whose presence we have detected in the past by ultrafast 2D HMBC experiments,[13c,20] but whose cross-peaks fall outside the window targeted here. Evolution of (**8**) by nucleophilic capture by acetonitrile-d_3 leads to the complex (**11**), which evolves to the nitrilium-salt intermediate (**12**).[21,22] The reaction continues, and an additional nucleophilic capture by the acetonitrile-d_3 takes place forming intermediate (**13**). In order to confirm these intermediates, measurements were repeated using labeled ^{13}C-methyl-acetophenone (**7**) and a standard UF-HSQC sequence,[23] which permits monitoring of (examination) an expanded acquisition window (4.50−0.50 ppm, ^{1}H; 63.60−3.60 ppm, ^{13}C). These results from monitoring of the methyl labeled reactant (**7**) confirmed the formation of intermediate (**8**) and its evolution to intermediates (**11**−**13**) (Figure 9).

Elimination of triflic anhydride from intermediate (**8**) would lead to vinyl triflate (**10**), which should form as a side product. Cross-peaks from (**10**) and/or from other possible olefinic intermediates like (**14**), however, were not observed in the HSQC of the olefinic window (5.17−6.50 ppm, ^{1}H; 106.0−

dx.doi.org/10.1021/ja210154g | J. Am. Chem.Soc. 2012, 134, 2706−2715

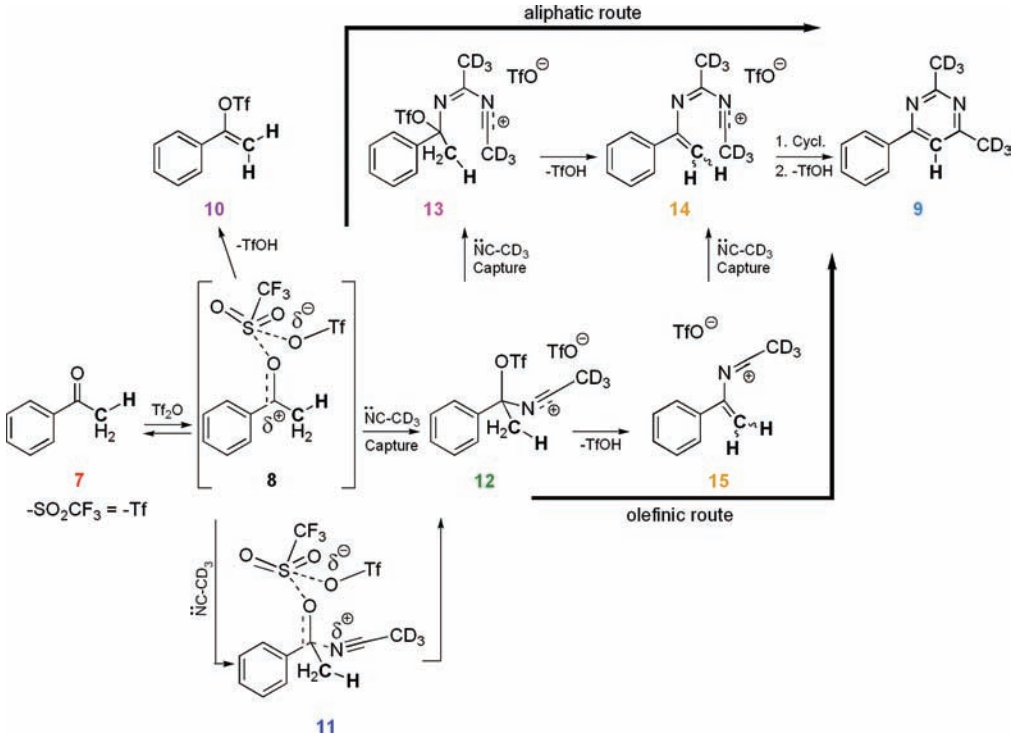

Figure 8. Proposed mechanism for the reaction of triflic anhydride, acetophenone (**7**), and acetonitrile-d_3 in accordance with the structural and kinetic insight gained from the ultrafast NMR experiments. The NMR results suggest two possible routes (an aliphatic and an olefinic) that can yield the final product (**9**) of the reaction.

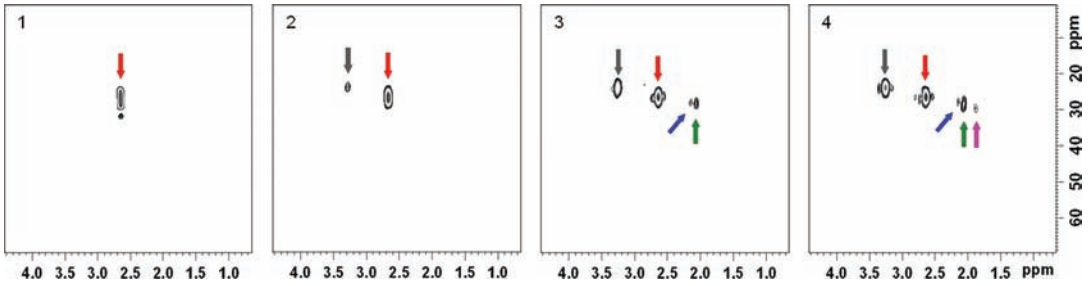

Figure 9. Representative series of real-time 2D HSQC NMR spectra recorded for the aliphatic window of a reaction between labeled ^{13}C-methyl-acetophenone (**7**, red arrow) with triflic anhydride and acetonitrile-d_3. From the crosspeaks detected by the UF-HSQC sequence in this spectral window, the formation of the intermediate (**8**, gray arrow) and its evolution to the intermediates (**11**, blue arrow), (**12**, green arrow), and (**13**, magenta arrow) can be monitored (see text for further information).

116.0 ppm, ^{13}C) starting from the unlabeled acetophenone (**7**). Still, intermediate (**14**) must also participate in the reaction,[7b] by elimination of triflic acid in intermediate (**13**). This would lead to the formation of the crucial double bond present in (**14**), in whose absence the cyclization step which leads to the pyrimidine ring cannot take place. Suspecting that these intermediates could not be seen due to a transient nature leading to maximal concentrations below our sensitivity limits, reactions were repeated using labeled ^{13}C-methyl-acetophenone (**7**) and the olefinic window revised with this aid (Figure 7). The results show the expected double cross-peaks from vinyl triflate (**10**) as well as a new pair of cross-peaks representing diastereotopic protons of a methylidene group (purple and dark-yellow arrows in Figure 7). We ascribe this new peak's origin to the triflate salt intermediates olefinic (**14**) and/or (**15**) containing two and one molecules of the nucleophilic acetonitrile-d_3, respectively. Cross-peaks from intermediates (**14**) and/or (**15**) are present since the first moments of the reaction (Figure 7); the formation of intermediate (**15**) would take place by the elimination of triflic acid from intermediate (**12**) and prior to a second nucleophilic capture by the acetonitrile-d_3 which leads to (**14**). The kinetic behavior of intermediates (**14**) and/or (**15**) (Figure 7) shows that these species form quickly and then decay, coexisting until the last moments of the reaction. Intermediate (**13**) (Figure 8) is the first step of the so-called aliphatic route,[13b] whereas intermediate (**15**) would be the first of the olefinic and (**14**) the common final intermediate. No unambiguous explanation for the cross-peak at 6.20/106.5 could be found; its presence under laboratory conditions was not detected.[14] The progress of the reaction through the aliphatic and/or olefinic route and the relative rate of both pathways will depend on the stability of intermediate (**12**).

Overall, the findings arising from these HSQC correlations reveal for the first time the presence of olefinic intermediates (**14**) and/or (**15**) and confirm preliminary results previously observed in ultrafast HMBC measurements where labeled reactants were used.[13c] In order to get further confirmation on

dx.doi.org/10.1021/ja210154g | J. Am. Chem.Soc. 2012, 134, 2706–2715

the nature of the detected intermediates, we exploited the valuable insight arising from the chemical shifts observed along the correlated ^{1}H and ^{13}C dimensions. Table 1 shows the

Table 1. Observed and Calculated Chemical Shifts of the Different Species Involved in the Reaction

	observed (CD_3CN)[a]		calculated ($CDCl_3$)[b]	calculated Gaussian 09[d]
	^{1}H	^{13}C	^{1}H	^{13}C
7	2.64	26.33	2.60	24,70[f]
		196.90		193.05[f] (216.00)[e]
8	3.26	23.71		28.75[e]
		195.2		202.40[e]
9[a,c]	8.33	119.01	6.85	123.02[e]
10	5.85	105.76	5.94	103.20[f] (118.60[e])
	5.49		4.50	
11	2.09	28.40		31.21[e]
12	2.01	28.05	1.64	33.60[e]
13	1.84	30.26	2.04	33.30[e]
14	5.89	114.50	5.08	110.70[e]
	5.54		4.97	
15	5.89	114.50	5.15	146.60[e]
	5.54		4.99	

[a]See the Supporting Information. [b]Averaged values of chemical shifts ACD/Laboratories (release 8.00). [c]Differences between observed and calculated chemical shifts are due to the nature of solvent. [d]Calculated with TMS (^{13}C = TMS value Gaussian 09 − value ^{13}C compound Gaussian 09). [e]Obtained with M06-2X approximation. [f]Obtained with B3LYP approximation.

experimental chemical shifts arising from the ultrafast series and compares them against expectations stemming from the various structures that are postulated to participate in the reaction scheme proposed in Figure 8. The ^{1}H NMR chemical shift estimations were performed for the nitrilium-salt intermediates (**12**−**15**), using the commercial chemical shift calculator software ACD/Laboratories (release 8.00). ^{13}C NMR shifts were calculated within the GIAO approximation on the PCM-M06-2X/6-31+G* (solvent = acetonitrile) with optimized geometries using the Gaussian 09 suite of programs. In all cases we find very good agreement between the observed values and the values predicted/calculated for the postulated structures; these calculations permit to distinguish between (**14**) and (**15**) and assign (**14**) to the triflic olefinic nitrilium-salt intermediate formed.

5. CONCLUSIONS

The real-time spectroscopic approaches herein described allowed us to uncover a new and interesting sequence of events in the mechanistic pathway of the alkylpyrimidine formation from aliphatic ketones and alkyl nitriles promoted by triflic anhydride. This was largely thanks to the advent of new ultrafast 2D NMR techniques that, operating under low gradients made possible by the use of selective band excitations, succeeded in monitoring the organic reaction using unlabeled compounds. Using this new selective and low-gradient-strength based UF sequence, it was possible to confirm the presence of intermediates reported in earlier studies such as (**8**) and (**14**) as well as intermediates (**11**−**13**) that were here detected for the first time. Estimations and calculations of NMR chemical shifts are in very good agreement with the proposed structures. These findings have permitted us to propose for the first time a new and complete mechanism involving two different and concurrent pathways—one aliphatic and the other olefinic—for the progress of the reaction. The evolution from the starting ketone to the final pyrimidine could be monitored and rationalized in high detail. In summary, we believe that real-time dynamic 2D NMR methodologies of the kind described in this work could open valuable new ways in the kinetic monitoring and characterization of complex dynamic chemical systems and in the elucidation of the variety of mechanisms underlying these transformations.

■ ASSOCIATED CONTENT

Supporting Information

Further details regarding experimental procedures, 1D and 2D spectra of products, and 3D animations. Complete ref 19. This material is free of charge via the Internet at http://pubs.acs.org.

■ AUTHOR INFORMATION

Corresponding Author

lucio.frydman@weizmann.ac.il; aherrera@quim.ucm.es

■ ACKNOWLEDGMENTS

The authors acknowledge financial support from MICINN (grant CTQ2010-14936), the Israel Science Foundation (ISF 447/09), ERC Advanced grant no. 246754, EU'S BioNMR grant no. 261863, a Helen and Kimmel Award for Innovative Investigation, and the generosity of the Perlman Family Foundation. G.O. acknowledges postdoctoral support from the Feinberg Graduate School (Dean Fellowship) and from the Fulbright Foundation. Z.P. acknowledges Universidad Complutense de Madrid for a predoctoral fellowship. We gratefully acknowledge Dr. Israel Fernández and Ángel Sánchez (UCM) for theoretical calculations and predictions of ^{13}C chemical shifts.

■ REFERENCES

(1) (a) Pozharskii, A. F.; Soldatenkov, A. T.; Katritzky, A. R. In *Heterocycles in Life and Society*; Wiley-VCH: Weinheim, Germany, 1997. (b) Eicher, T.; Hauptmann, S. In *The Chemistry of Heterocycles*, 2nd ed.; Wiley-VCH: Weinheim, Germany, 2003. (c) Katritzky, A. R. In *Advances in Heterocyclic Chemistry*; Academic Press: Oxford, U.K., 2002; Vol.82.

(2) Rewcastle, G. W. In *Comprehensive Heterocyclic Chemistry III*; Aitken, A., Ed.; Elsevier Science: Oxford, U.K., 2008; Vol, *8*, pp117. Ahmad, O. K.; Hill, M. D.; Movassaghi, M. *J. Org. Chem.* **2009**, *74*, 8460−8463.

(3) (a) von Angerer, S. In *Science of Synthesis*; Yamamoto, Y., Ed.; Thieme: Stuttgart, Germany, 2003; Vol. *16*, pp 379. (b) Hill, M. D.; Movassaghi, M. *Chem.−Eur. J.* **2008**, *14*, 6836−6844.

(4) (a) Herrera, A.; Martínez-Álvarez, R.; Ramiro, P.; Molero, D.; Almy, J. *J. Org. Chem.* **2006**, *71*, 3026−3032. (b) Herrera, A.; Martínez-Álvarez, R.; Martín, N.; Chioua, M.; Chioua, R.; Sánchez-Vázquez, Á.; Molero, D.; Almy, J. *Tetrahedron* **2009**, *65*, 1697−1703. (c) Herrera, A.; Martínez-Álvarez, R.; Martín, N.; Chioua, M.; Chioua, R.; Sánchez-Vázquez, Á.; Molero, D.; Almy, J. *Tetrahedron* **2009**, *65*, 5817−5823. (d) Herrera, A.; Martínez-Álvarez, R.; Ramiro, P.; Sánchez, A.; Torres, R. *J. Org. Chem.* **2004**, *69*, 4545−4547. (e) Martínez-Álvarez, R.; Herrera, A. *Targets Heterocycl. Syst.* **2008**, *12*, 59−85.

(5) (a) Movassaghi, M.; Hill, M. D. *J. Am. Chem. Soc.* **2006**, *128*, 14254−14255. (b) Movassaghi, M.; Hill, M. D. *J. Am. Chem. Soc.* **2006**, *128*, 4592−4593. (c) Hill, M. D.; Movassaghi, M. *Synthesis* **2007**, 1115−1119. (d) Movassaghi, M.; Hill, M. D. *Nat.Protoc.* **2007**, *2*, 2018−2023. (e) Ahmad, O. K.; Hill, M. D.; Movassaghi, M. *J. Org. Chem.* **2009**, *74*, 8460−8463. (f) Menor-Salvan, C.; Ruiz-Bermejo, M.;

Guzmán, G. I.; Osuna-Esteban, S.; Veintemillas-Verdaguer, S. *Chem.–Eur. J.* **2009**, *15*, 4411–4418. (g) Bannwarth, P.; Vailleix, A.; Gree, D.; Gree, R. *J. Org. Chem.* **2009**, *74*, 4646–4649. (h) Yan, S.; Tang, Y.; Yu, F.; Lin, J. *Helv. Chim. Acta* **2011**, *94*, 487–490. (i) Lin, M.; Chen, Q-z.; Zhu, Y.; Chen, X-l.; Cai, J-j.; Pan, Y-m.; Zhan, Z-p. *Synlett* **2011**, 1179–1183.

(6) Lai, P-S; Taylor, M. S. *Synthesis* **2010**, 1449–1452.

(7) (a) García Martínez, A.; Herrera Fernández, A.; Moreno Jiménez, F.; García Fraile, A.; Subramanian, L. R.; Hanack, M. *J. Org. Chem.* **1992**, *57*, 1627–1630. (b) Herrera, A.; Martínez-Álvarez, R.; Chioua, M.; Chioua, R.; Sánchez, Á. *Tetrahedron* **2002**, *58*, 10053–10058. Chemical transformations induced by triflic anhydride were reviewed, see: (c) Baraznenok, I. L.; Nenajdenko, V. G.; Balenkova, E. S. *Tetrahedron* **2000**, *56*, 3077–3119.

(8) (a) Kupce, E.; Nishida, T.; Freeman, R. *Prog. Nucl. Magn. Reson. Spectrosc.* **2003**, *42*, 95–122. (b) Kupce, E.; Freeman, R. *J. Magn. Reson.* **2003**, *162*, 300–310.

(9) Hoch, J. C.; Stern, A. S. *Method Enzymol.* **2001**, *338*, 159–78.

(10) (a) Gal, M.; Frydman, L. In *Multidimensional NMR methods for the Solution State*; Morris, G. A., Emsley, J. W., Eds.; Wiley&Sons: Chichester, U.K., 2010; pp 43–60. (b) Mishkovsky, M.; Frydman, L. *Annu. Rev. Phys. Chem.* **2009**, *60*, 429–448.

(11) Frydman, L.; Scherf, T.; Lupulescu.. *Proc. Natl. Acad. Sci. U.S.A.* **2002**, *99*, 15958–15862.

(12) (a) Gal, M.; Schanda, P.; Brutscher.; Frydman, L. *J. Am. Chem. Soc.* **2007**, *129*, 1372–1377. (b) Gal, M.; Lee, M. K.; Varani, G.; Frydman, L. *Proc. Natl. Acad. Sci. U.S.A.* **2010**, *107*, 9192–9197.

(13) (a) Gal, M.; Mishkovsky, M.; Frydman, L. *J. Am. Chem. Soc.* **2006**, *128*, 951–956. (b) Herrera, A.; Fernández-Valle, E.; Martínez-Álvarez, R.; Molero, D.; Pardo, Z. D.; Sáez, E.; Gal, M. *Angew. Chem., Int. Ed.* **2009**, *48*, 6274–6277. (c) Herrera, A.; Fernández-Valle, E.; Gutiérrez, E. M.; Martínez-Álvarez, R.; Molero, D.; Pardo, Z. D.; Sáez, E. *Org. Lett.* **2010**, *12*, 144–147.

(14) (a) Pelupessy, P.; Duma, L.; Bodenhausen, G. *J. Magn. Reson.* **2008**, *194*, 169–174. (b) Shrot, Y.; Frydman, L. *J. Chem. Phys.* **2009**, *131*, 224516/1–224516/11. (c) Giradeau, P.; Shrot, Y.; Frydman, L. *J. Am. Chem. Soc.* **2009**, *131*, 13902–13903. (d) Giradeau, P.; Akoka, S. *J. Magn. Reson.* **2010**, *205*, 171–176.

(15) Brunner, P.; Ernst, R. R. *J. Magn. Reson.* **1979**, *33*, 83–106.

(16) Wolinski, K.; Hinton, J. F.; Pulay, P. *J. Am. Chem. Soc.* **1990**, *112*, 8251–8260.

(17) M06–2X method: Zhao, Y.; Truhlar, D. G. *Acc. Chem. Res.* **2008**, *41*, 157–167.

(18) PCM method: (a) Miertus, S.; Scrocco, E.; Tomasi, J. *Chem. Phys.* **1981**, *55*, 117–129. (b) Pascual-Ahuir, J. L.; Silla, E.; Tuñón, I. *J. Comput. Chem.* **1994**, *15*, 1127–1138. (c) Barone, V.; Cossi, M. *J. Phys. Chem. A* **1998**, *102*, 1995–2001.

(19) Frisch, M. J. et al. *Gaussian 09*, revision B.01, Gaussian, Inc.: Wallingford, CT, 2009.

(20) ^{13}C NMR data for carbocations: (a) Breitmeier, E.; Voelter, W. In *Carbon-13 NMR Spectroscopy*, 3rd ed.; VCH: New York, 1987. (b) Stadler, D.; Goeppert, A.; Rasul, G.; Olah, G. A.; Prakash, S.; Bach, T. *J. Org. Chem.* **2009**, *74*, 312–318.

(21) Kanemasa, S. In *Science of Synthesis*; Murahashi, S., Ed.; Thieme: Stuttgart, 2001; Vol *19*, pp 53–65.

(22) (a) Darbeau, R. W.; Gibble, R. E.; Pease, R. S.; Bridges, D. E.; Siso, L. M.; Heurtin, D. J. *J. Chem. Soc., Perkin Trans. 2* **2001**, 1084–1090. (b) White, E. H.; DePinto, J. T.; Polito, A. J.; Bauer, I.; Roswell, D. F. *J. Am. Chem. Soc.* **1988**, *110*, 3708–3709.

(23) Shrot, Y.; Shapira, B.; Frydman, L. *J. Magn. Reson.* **2004**, *171*, 163–170.